X-ray Absorption Spectroscopy of Titanium Oxide by Time Dependent Density Functional Calculations

G. Fronzoni,*,†,‡,§ R. De Francesco,†,‡,§ M. Stener,†,‡,§ and M. Causà||

Dipartimento di Scienze Chimiche, Via L. Giorgieri 1, Università di Trieste, I-34127 Trieste, Italy, Consorzio Interuniversitario Nazionale per la Scienza e Tecnologia dei Materiali, INSTM, Unita' di Trieste, INFM DEMOCRITOS National Simulation Center, Trieste, Italy, and Dipartimento di Scienze dell'Ambiente e della Vita, Università del Piemonte Orientale, Via V. Bellini 25/G, 15100 Alessandria, Italy

Received: December 16, 2005; In Final Form: March 14, 2006

The potentiality of the time dependent density functional theory (TDDFT) for the description of core excitation spectra (XAS) in transition metal oxides is analyzed, considering the rutile form of TiO_2 as a test case. Cluster models are adopted to mimic the bulk, embedded within an array of point charges to simulate the Madelung potential. All of the edges, titanium and oxygen K and titanium L edges, are considered, and the TDDFT results are compared with the experimental data in order to assess the performance of the theoretical approach in dealing with this complex class of compounds. Satisfactory results have been obtained for the Ti and O K edges, while in the case of the Ti L edge some discrepancies with the experiment are still present. The configuration mixing explicitly included in the TDDFT model strongly influences the distribution of the 2p metal oscillator strength. The origin of the spectral features is investigated with the help of the partial density of the virtual states (PDOS) calculated for each core hole considered, which can be qualitatively compared with the theoretical spectra calculated in the Kohn−Sham one-electron approach.

1. Introduction

X-ray absorption spectroscopy (XAS) is a local process in which a core electron is promoted to an excited electronic state; therefore, the observed spectral structures near the ionization threshold (NEXAFS region) are closely related to the local electronic structure around the atom in which the excitation takes place and contain significant information on the low-lying unoccupied states of the systems. The intensity of the excitation process is related to the coupling between the initial core state and the excited state by the electric dipole selection rule; therefore, it maps the dipole-allowed atomic site component of the final virtual state. From an experimental point of view, the most recent integration between the electron energy loss (EELS) techniques and the transmission electron microscope (TEM)[1,2] has improved the studies in condensed matter also at the nanoscale level and has renewed the attention on theoretical approaches suited for the reproduction and interpretation of the experimental data in terms of the electronic structure of the sample. The interpretation of the EELS spectra of condensed systems requires first principle calculations, and although many efforts have been spent to reproduce the spectra, a robust and general method has not yet emerged clearly. It has been verified that a single particle description of the XAS spectra generally works well for the K edges and several dedicated computer codes exist;[3] for other edges, in particular the transition metal L edge, coupling between configurations has to be included in the computational scheme for a realistic description of the core spectrum. In this respect, the time dependent density functional theory (TDDFT) represents an essential improvement over the single particle approaches and appears therefore to be a suitable compromise between accuracy and computational economy needed to treat large systems. Current TDDFT implementations allow valence electron excitations to be described, providing a good accuracy for molecular systems. Only more recently it has been applied also to the treatment of the optical transitions of defects in solids using suitable cluster model approaches.[4−7] The recent extension of the TDDFT method for the treatment of the core electron excitations has proven to be reliable to reproduce and give interpretation of core absorption spectra both in simple and in more complex molecules.[8,9] Furthermore, it has also been applied to the calculations of core excitations of the series of alkaline-earth oxides (from MgO to BaO),[10,11] using a cluster model to mimic the bulk of the oxides. All of the edges (metal 1s and 2p and oxygen 1s) have been considered, obtaining good agreement with the available experimental data. The reliability of the TDDFT computational method employed in ref 11 to describe the XAS spectra of solid samples may be twofold. One reason is that a finite cluster model should be advantageous for the calculation of core excitations, since the excited electron is localized near the core hole; therefore, the description of a limited region would be sufficient to describe it accurately. The second one is the potentiality of the TDDFT approach, which formally includes the coupling between single configurations and therefore overcomes the limitations of single particle approaches. It allows to describe in particular situations in which the core state is degenerate, like in 2p orbitals, and also degenerate final atomic *n*d contributions are accessible.

It would be particularly meaningful to extend the study to transition metal oxides which remain one of the most difficult classes of solids on which to perform spectroscopic property predictions through ab initio calculations. In fact, while a single particle description of the X-ray absorption generally works well for the metal and oxygen K edges, the agreement is poor for

* Corresponding author. E-mail: fronzoni@univ.trieste.it.
† Dipartimento di Scienze Chimiche, Università di Trieste.
‡ INSTM, Unita' di Trieste.
§ INFM DEMOCRITOS National Simulation Center.
|| Università del Piemonte Orientale.

10.1021/jp057353a CCC: $33.50
Published on Web 05/03/2006

the metal L edge, due to the strong overlap of the 2p core hole with the 3d electrons which requires the inclusion of configuration mixing in the theoretical approach. The L edge is particularly rich in information and for transition metal compounds is associated with the p → d dipole transitions which directly probe the metal d participation to the virtual states, therefore detailing the d involvement in the bonding.

In this work, the TDDFT is applied to the calculations of the core excitation spectra of the bulk titanium dioxide (TiO_2) in its most common polymorphic form, the rutile structure. In the rutile structure, each Ti atom is surrounded by a slightly distorted octahedron of O atoms. Its electronic structure has been extensively investigated experimentally by core level spectroscopies such as electron energy loss spectroscopy (EELS) and X-ray absorption spectroscopy (XAS).[12−20] Several theoretical calculations, in particular on the Ti and O K edges, have been performed, both adopting a band structure and cluster methods;[21−27] however, only in the study of ref 17 are all of the edges investigated using the same computational approach. Therefore, TiO_2 represents an interesting test case to assess the performance of the TDDFT scheme for the reproduction of core excitation spectra in the complex case of transition metal oxides. The present study considers all of the possible core edges, namely, the Ti K edge, the Ti L edge, and the O K edge which are investigated at the same level of accuracy and compared with the experimental measurements. Also, the partial density of unoccupied states relative to the each core hole is considered, to find a clearer interpretation of the calculated spectral features in terms of the dominant contribution of the atomic orbitals to the final virtual molecular orbitals.

2. Theoretical Method

The TDDFT approach for electron excitations and its implementation in the ADF code have been described in detail in the literature,[28,29] so here, we just recall the salient steps and describe the new features. The general problem is cast in the following eigenvalue equation:

$$\mathbf{\Omega F}_i = \omega_i^2 \mathbf{F}_i \tag{1}$$

where $\mathbf{\Omega}$ is a four-index matrix with elements $\Omega_{ia\sigma,jb\tau}$; the indexes consist of products of occupied-virtual (ia and jb) Kohn−Sham (KS) orbitals, while σ and τ refer to the spin variable. The eigenvalues correspond to squared excitation energies, while the oscillator strengths are extracted from the eigenvectors $\mathbf{F}_i$.[28] The Ω-matrix elements can be expressed in terms of KS eigenvalues (ϵ) and the coupling matrix $\mathbf{K}$:

$$\Omega_{ia\sigma,jb\tau} = \delta_{\sigma\tau}\delta_{ij}\delta_{ab}(\epsilon_a - \epsilon_i)^2 + 2\sqrt{(\epsilon_a - \epsilon_i)}\sqrt{(\epsilon_b - \epsilon_j)}K_{ia\sigma,jb\tau} \tag{2}$$

The elements of the coupling matrix $\mathbf{K}$ are given by

$$K_{ia\sigma,jb\tau} = \int d\mathbf{r} \int d\mathbf{r}'\, \varphi_{i\sigma}(\mathbf{r})\, \varphi_{a\sigma}(\mathbf{r})\left[\frac{1}{|\mathbf{r}-\mathbf{r}'|} + f_{xc}^{\sigma\tau}(\mathbf{r},\mathbf{r}',\omega)\right]\varphi_{j\tau}(\mathbf{r}')\, \varphi_{b\tau}(\mathbf{r}') \tag{3}$$

where φ are the KS orbitals and $f_{xc}^{\sigma\tau}(\mathbf{r},\mathbf{r}',\omega)$ is the exchange-correlation kernel. In this work, the kernel is approximated according to the adiabatic local density approximation (ALDA).[30]

The space spanned by the solutions of the eigenvalue equation (eq 1) corresponds to the 1h−1p excited configurations, so it is possible to approximate this space operating a selection over the configurations, keeping only those necessary for an accurate description of the phenomenon, as is customary in ab initio CI (Configuration Interaction) calculations. Thus, in practice, according to the method in ref 8, the indexes which span the occupied orbital space (i and j) are limited to run only over the core shell.

KS calculations have also been performed, to evaluate the effect of configuration mixing introduced at the TDDFT level. In the KS scheme, the oscillator strengths are calculated directly as the dipole transition moments between the KS one-electron eigenfunctions and the excitation energies as eigenvalue differences.

The partial density of states (PDOS) calculations have been performed in order to provide a pictorial representation of Mulliken populations related to the virtual molecular orbitals of the clusters. In particular, to find out if a given atomic function χ_μ contributes strongly to molecular orbitals at certain energies, one may weight the different one-electron levels by using the percentage χ_μ character. If the χ_μ character is determined by the gross populations, the gross population density of states form of the PDOS is then obtained:

$$N_\mu(E) = \sum_i \mathrm{GP}_{i,\mu} L(E - \epsilon_i) \tag{4}$$

where the index i runs over the one-electron energy levels, ϵ_i is the energy of the ith level, $L(E - \epsilon_i)$ is a Lorentzian function of appropriate full width at half-maximum (fwhm), and $\mathrm{GP}_{i,\mu}$ is the gross population of the χ_μ function in a specific orbital density $|\phi_i(\bar{r})|^2$:

$$\mathrm{GP}_{i,\mu} = \sum_\nu P_{i,\mu\nu} S_{\mu\nu} = \sum_\nu C_{\mu i} C_{\nu i} S_{\mu\nu} \tag{5}$$

where $S_{\mu\nu}$ is the overlap matrix between the χ_μ and χ_ν basis functions and $C_{\mu i}$ are the coefficients of the χ_μ function in the ith molecular orbital (MO). In this way, $\mathrm{GP}_{i,\mu}$ is associated with the fraction of the orbital density belonging to that function (percentage χ_μ character of the MO ϕ_i).

3. Computational Details

The calculations have been performed with the ADF program (version 2003.01)[31,32] modified according to the previous section. Basis sets of DZP type, consisting of STO functions, have been employed. The adequacy of the DZP basis set size if the cluster size is sufficiently large has been demonstrated in previous works on alkaline-earth oxides.[10,11] The frozen core (FC) computational technique has been used in order to reduce the computing time without losing accuracy. It consists of treating explicitly only electrons in the outer levels, while the innermost atomic shells (core) are kept frozen. The following basis set scheme has been adopted:

Ti	FC 3p	core 9s 4p/outer 2s 1p 4d
O	FC 1s	core 5s/outer 2s 2p 1d

The all-electron basis set is used only for the excited atom. For the calculation of the Ti K and L edges, only one Ti atom, lying at the center of the cluster, is excited, while, for the calculation of the O K edge, six O atoms, lying in a distorted-octahedron configuration around the Ti central atom, are excited (see below for the cluster description).

A closed-shell electronic structure has been assumed by considering a fully ionic configuration, formally described by Ti^{4+} and O^{2-} ions.

The LB94[33] exchange-correlation potential with the ground state (GS) electron configuration has been employed. It has been chosen because of its correct asymptotic behavior, which is a necessary condition for a good description of virtual orbitals. The SAOP exchange-correlation potential is also characterized by a correct asymptotic behavior, and its performance for the description of the XAS spectra has been tested in a previous work;[8] the comparison with the LB94 results has not revealed apparent dependency from the potentials, apart from a large shift in the absolute energy scale, due to the strong underestimate of the SAOP excitation energies with respect to the experimental values. It has been pointed out in the literature[34,35] that the inclusion of core hole effects in cluster calculations is essential for a good reproduction of XAS spectra, in particular for the K edge, to account for the charge rearrangement occurring in the response of core hole formation. These are final state effects associated with the many-body character of the wave function, and they can be introduced in the calculation both explicitly through the use of relaxed orbitals to describe the final states, as in the ΔSCF scheme, and through the configuration mixing. In the case of the TDDFT formalism, the configuration mixing is explicitly included only at one-hole one-particle (1h−1p) level, although higher excitation levels can be in principle included indirectly within the exchange-correlation response kernel.[28] In the present case, we are confident that the ALDA employed to represent the exchange-correlation kernel is not actually able to recover relaxation effects via higher-energy order excitations. On the other hand, previous experience on core hole ionization, where relaxation is even more important than in the core excitations,[36,37] has indicated the good performances of the LB94 exchange-correlation potential both at the KS[36] and TDDFT[37] levels. Moreover, we have tested in our previous work on MgO[10] the VWN potential[38] with the transition state (TS) configuration, which consists of removing half an electron from the core orbital, to assess the importance of core hole relaxation, which is not accounted for with the GS configuration of the LB94 potential. Only minor differences with respect to the LB94-GS results have been observed in the lower-energy region, in particular an increase of the pre-edge intensity at the Mg K edge using the VWN-KS scheme. However, the inclusion of response effects through the TDDFT formalism appears more important for the quality of the results, in particular in the case of degenerate edges.

The exchange-correlation kernel is approximated within the usual ALDA scheme, and only excitations with singlet spin symmetry have been considered, since all of the clusters have a closed-shell electronic structure.

As concerns the simulation of the bulk rutile structure, we have to consider that in its tetragonal structure each titanium atom is coordinated to six oxygen atoms, forming an octahedron which is slightly distorted, with two Ti−O distances being slightly greater than the other four. This lowers the local symmetry around the titanium atom from O_h to D_{2h}. The cluster models employed in this study are built by extracting a proper set of atoms from the experimental lattice of rutile, using the following experimental values for the crystallographic parameters: $a = b = 4.5930$ Å, $c = 2.9590$ Å.[39] The clusters have been built by setting at the center a Ti atom and then adding progressive shells of Ti and O atoms, following the scheme of Sousa et al.;[40] in this way, a series of clusters has been obtained (we report some of them in Figure 1), with the largest cluster $[Ti_{15}O_{40}]^{20-}$ made of 55 atoms.

To better simulate the bulk situation, the clusters have been embedded within an array of point charges (PCs), whose optimized values are taken from the reference of Sousa et al. used also to obtain the atomic coordinates.[40] Following that scheme, the cluster $[TiO_6]^{8-}$ is embedded within an array of 470 PCs, and for larger clusters, successive shells of PCs are substituted by Ti and O atoms, respectively, so that the cluster $[Ti_{15}O_{40}]^{20-}$ is embedded within an array of 422 PCs; the sum of the cluster nuclearity and the PCs number is constant and equal to 477. The cluster charge plus PCs makes substantially a neutral object with deviations less than 0.23 au for the largest cluster. The use of this set of PCs forces the symmetry of the system to lower from D_{2h} (the real symmetry of rutile) to C_{2h}, because of the presence of PCs that are equivalent for their positions but not for their absolute values.

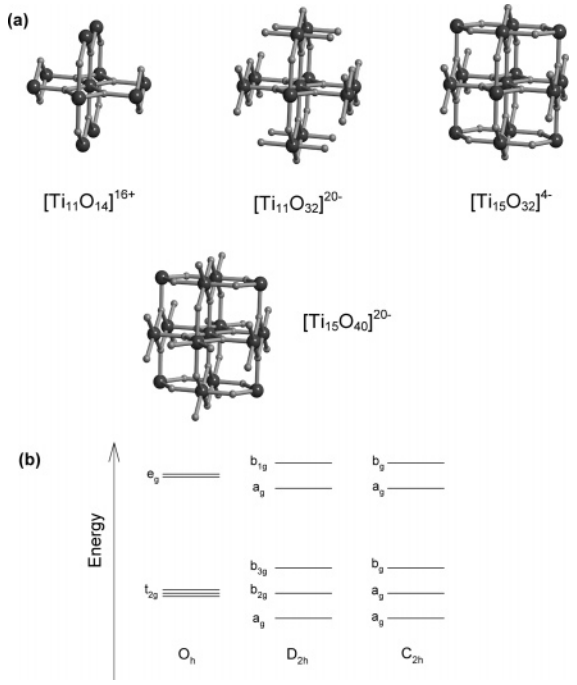

Figure 1. (a) Cluster models employed in the present work. Large, dark balls represent Ti atoms, and small, light balls represent O atoms. For all clusters, the excited titanium is the central one, while the excited oxygens are the six O atoms surrounding the central Ti atom. (b) Diagram of symmetry splitting of d orbitals in O_h, D_{2h}, and C_{2h} point groups.

The use of embedding in terms of PCs is a simple but efficient way to describe the Madelung potential in ionic materials. It has been discussed for surface cluster models in ref 41 and analyzed for various phenomena with respect to the size of the cluster. In particular, the study suggests that the inclusion of the long range Coulombic interactions is essential when the clusters are small. The importance of using PCs to describe cluster models which simulate the bulk of alkaline-earth oxides has been observed as decisive in our previous works;[10,11] in particular, the clusters in the absence of embedding in general give rise to unphysical open-shell structures which are not suitable to model the bulk situation. The use of PCs could be less obvious for materials in which the bonding has a mixed ionic−covalent character, like in TiO_2, [41] and may depend on the properties of interest. The series of clusters designed to represent the TiO_2 bulk has allowed the evolution of the calculated XAS spectra with the size of the cluster to be followed (both Ti 1s and Ti 2p spectra have been calculated for the series), and therefore with the long range effect of the external potential. This analysis has shown that the $[Ti_{15}O_{40}]^{20-}$ cluster is suitable for a realistic description of the core excitation of the Ti central metal atom. When the convergence of the

spectral features is reached, the dimension of the cluster is considered sufficiently large to ensure a substantial independency of the calculated spectroscopic properties on the external potential represented with PCs.

The cluster $[Ti_{15}O_{40}]^{20-}$ is built up by setting three shells of Ti atoms and eight shells of O atoms around the central Ti atom. The calculation of Ti 1s and 2p core excitations is straightforward, because only the central Ti atom of the cluster has to be excited. The calculation of the O K edge spectrum requires instead the excitation of the core electrons of the six oxygen atoms surrounding the central Ti (see Figure 1). These six atoms are grouped into four equivalent "equatorial" atoms (distance Ti−O = 1.93 Å) and two equivalent "apical" atoms (distance Ti−O = 2.01 Å). For the sake of computational efficiency, the most convenient choice is to excite the four equatorial and two apical oxygens separately and then superimpose the two excitation spectra (equatorial and apical), obtaining the final O K edge spectra. This procedure is correct only if there is no coupling between the nonequivalent oxygen atoms. This has been verified performing a calculation of the O K edge spectrum obtained by promoting the excitation of the six O atoms in the same step. These test calculations have been performed using the intermediate $[Ti_{11}O_{14}]^{16+}$ cluster (see Figure 1), and the results obtained show that the spectra obtained with the two different procedures are substantially equivalent.

The calculated spectra have been convoluted with Gaussian functions in order to facilitate the comparison with the experiments, while the calculated DOS profiles have been convoluted employing Lorentzian functions. The fwhm values employed are reported in the captions of the figures.

4. Results and Discussion

The TiO_2 oxide has a nominally $3d^0$ ground state configuration which would correspond to a fully ionic limit. However, as a result of the Ti−O covalent interaction, the Ti 3d band contains a contribution from the O 2p orbitals (usually referred to as the O 2p band at lower energy) and, at the same time, a small contribution of Ti 3d orbitals is present in the O 2p bonding states. If we consider the simplest cluster representation of a titanium atom surrounded by six oxygen nearest neighbors $[TiO_6]^{8-}$, then we obtain a schematic diagram of the lowest unoccupied MOs, as reported in Figure 1 (panel b). In octahedral O_h symmetry, the crystal field splitting separates the two lowest unoccupied levels (mostly Ti 3d with some O 2p character) into two groups: the 3-fold t_{2g} and 2-fold e_g. The lowering of the symmetry to D_{2h} causes both of these levels to split as shown. Higher in energy are the a_{1g} and t_{1u} antibonding orbitals which represent the virtual counterpart of the completely filled bonding combination between the Ti 4sp states and the O 2p states. When considering the cluster model $[Ti_{15}O_{40}]^{20-}$ employed in the present work, it is convenient to refer to the partial density of the unoccupied states (PDOS) in order to analyze the nature of the virtual states. Figure 2 (panel a) reports the PDOS (*n*s, *n*p, and *n*d for Ti and *n*p for O) for this cluster; the PDOS refers to the sum of all *n* orbital components provided by the basis set employed, therefore allowing a clear representation of the various contributions of the atomic orbitals (AOs) to the virtual molecular orbitals (MOs). As we can see, the nature of the virtual orbitals agrees with the previous description of the electronic structure: the low-lying virtual MOs are dominated by the Ti 3d component with a significant O 2p participation, confirming the mixing of the Ti 3d and O 2p orbitals in the conduction band. The titanium *n*s and *n*p components give contributions to the virtual states at higher energy, where also

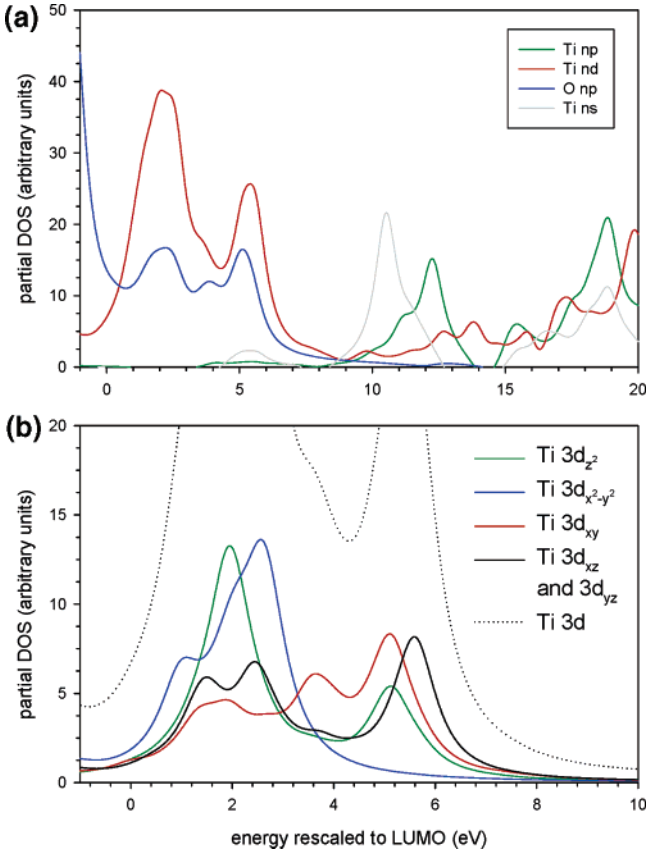

Figure 2. Partial DOS profiles vs the energy of the calculated electronic levels of the cluster $[Ti_{15}O_{40}]^{20-}$ embedded in an array of 422 PCs. Energy is rescaled with respect to the LUMO KS energy value, which is taken as zero; the absolute LUMO energy is −10.489 eV. DOS profiles are convoluted with Lorentzian functions (fwhm = 1.0 eV). (a) Ti s-, p-, and d- and O p-PDOS profiles. (b) Enlargement of the Ti d-PDOS region; the different d contributions are highlighted.

the higher metal *n*d components (in particular 4d) are present. In the present work, the PDOS results will be used as a support for the interpretation of the calculated spectral features in terms of the dominant contributions of the atomic orbitals in the final state. In fact, in a single particle approximation, it can be assumed that the core excitations are related to the unoccupied partial density of states of the selected atom that is allowed by the electric dipole selection rule.

In the following discussion the theoretical spectra will be compared with experimental data. In this respect, it is more convenient to consider the relative energy shift among the structures than the absolute scale, and therefore, the experimental profiles are shifted to the calculated ones so as to make the best match. It has been pointed out in ref 42 that for a computed XAS spectrum possible errors in the functionals may lead to an overall shift of the spectrum, while the relative energy positions are significantly less affected. In each theoretical spectrum, the calculated ionization limit is reported. This is important to identify the spectral features lying above the threshold which have to be considered with caution. In fact, the virtual final orbitals above edge are unbound and the LCAO-MO approach in a finite basis set is not capable of properly describing them. Only when the coupling between the discrete virtual orbitals generated by the present approach and the nonresonant continuum, not included, is weak it can be assumed that the discrete transitions calculated above edge may afford a qualitative estimate of the shape resonances observed in the cross section, at least in the lower-energy range. For this reason, we

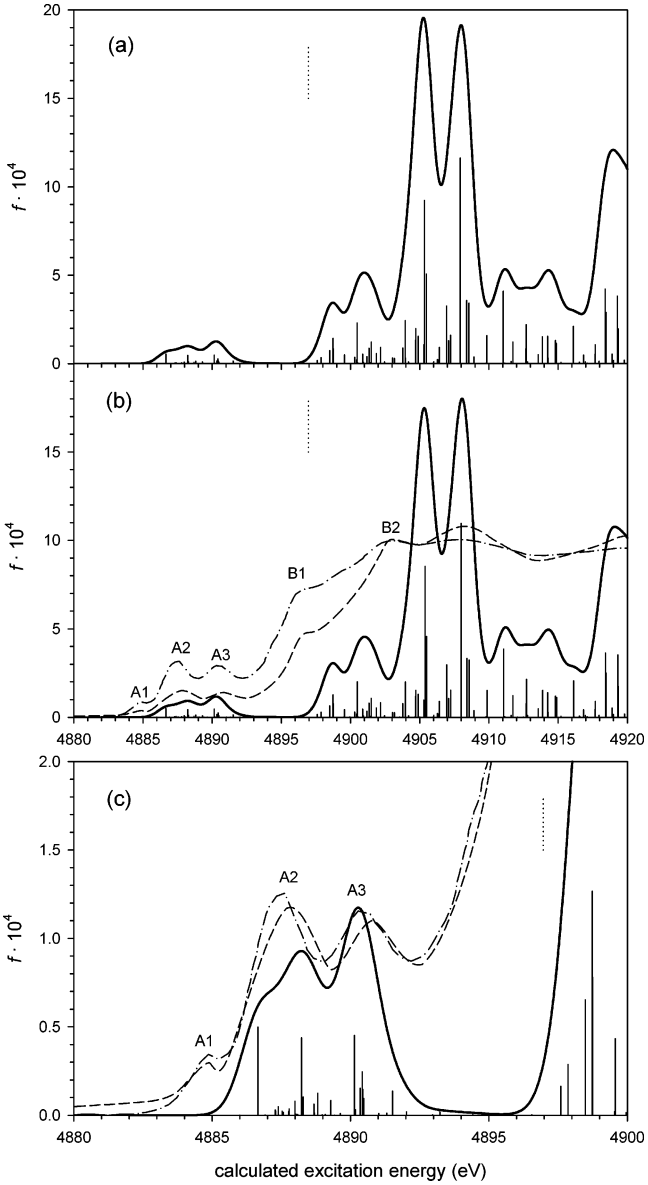

Figure 3. Ti 1s excitation spectra for the cluster $[Ti_{15}O_{40}]^{20-}$ embedded in an array of 422 PCs. Vertical dotted line: DFT-KS ionization threshold (opposite eigenvalue): 4896.961 eV. Excitation profiles are convoluted with Gaussian functions (fwhm = 1.5 eV). (a) Solid line, KS spectrum. (b) Solid line, TDDFT spectrum; dash−dotted line, experiment;[17] dashed line, experiment.[43] (c) solid line, TDDFT spectrum, pre-edge region; experimental profiles, see panel b.

consider only the theoretical results relative to an energy range extending up to about 20 eV above the calculated ionization limit.

4.1. Metal K Edge Spectrum. Several experimental investigations of the Ti K edge spectrum by X-ray absorption spectroscopy and electron energy loss spectroscopy are present in the literature; we report only the experimental data from refs 17 and 43 in Figure 3 for comparison with the TDDFT calculated spectrum (lower panel). The experimental spectrum[17] shows well resolved structures: three weak pre-edge peaks (labeled A1, A2, and A3) followed by features (labeled B1, B2, B3, and B4) on the higher-energy part of the rising edge. The origin of the three pre-edge features has been largely debated, and different explanations have been proposed in the literature.[14,15,17,21,25,44,45] Experimental studies based on the angular dependence of the XAS spectrum of the Ti K edge[15,46] have indicated the sensitivity of the A1 peak, and to a lesser extent of the A2 peak, to the orientation in a way characteristic of a quadrupolar transition. The parallel absence of any angular dependence of the A3 peak has been assigned to a purely dipolar origin. This analysis is supported by a recent experimental study of the resonant Auger spectrum taken at the Ti K edge,[47] which allows the dipolar and quadrupolar contributions in the pre-edge region to be resolved as being distinct Auger peaks. The experimental data have been reproduced by different theoretical approaches which consider both dipolar and quadrupolar transitions in the calculations as well as the polarization dependence of the spectra.[23,48,49] These studies explain that the A1 peak is only quadrupolar ($1s \rightarrow 3d\ (t_{2g})$), the A2 peak is dipolar in nature but includes also a little quadrupolar component ($1s \rightarrow 3d\ (e_g)$), while the A3 peak is a pure dipolar component.

The present calculated TDDFT spectrum models correctly the major spectral features, both in the below edge region and above the ionization limit. Our calculations do not consider the treatment of the quadrupole transitions; therefore, the present interpretation is based on the dipole selection rule. This allows transitions from the Ti 1s core orbital to unoccupied orbitals with contribution from p atomic components of the central metal atom which is expected to be mapped by the calculated oscillator strength *f*. The partial density of virtual states reported in Figure 2 shows that the Ti p contribution to the low-lying final states, of mainly Ti 3d character, is very low, and this can be related to the small intensity of the pre-edge features calculated at the TDDFT level. The TDDFT features are associated to transitions toward orbitals with mainly metal 3d character of the higher shell Ti atoms which can mix with the 4p orbitals of the absorbing atom, on the basis of symmetry consideration, in agreement with previous attributions.[21] In particular, the 3d orbitals of the Ti atoms are split by the crystal field essentially into two manifolds, often indicated as t_{2g}- and e_g-like molecular orbitals, which are substantially maintained in the lowest D_{2h} and C_{2h} symmetry, as suggested by the orbital diagram sketched in Figure 1. This accounts for the calculated double-peaked structure which correctly describes the A2 and A3 experimental features, in particular as concerns its energy width, which is about 3.6 eV in the calculation (3.1 eV in the experiment[17]).

The weak A1 lower-energy peak observed in the experiment, and attributed to the $1s \rightarrow 3d\ (t_{2g})$ quadrupolar transition as before emphasized, is absent in our calculated spectrum. Since the present computational scheme includes only dipolar transitions, the TDDFT results could indirectly support such a hypothesis. As concerns the structures above the ionization threshold, a qualitative agreement between the TDDFT results and the experimental data is found, although the theoretical features tend to be too sharp with respect to the experimental profile, due to an artifact of the continuum discretization explained in the previous paragraph. A slight overestimate of the energy separation between the features calculated below and above the ionization threshold is also observed with respect to the experimental profile. The calculated transitions are toward final states of p character from the neighboring Ti atoms with important contributions also from the 4p orbital of the central Ti atom, and this is responsible for the increase of the intensity of these transitions with respect to the below edge ones. The distribution of the p components relative to the central Ti atom in the PDOS of Figure 2 accordingly shows the increase of the metal p contribution at the higher-energy side of the 3d metal region. In particular, the first two small peaks calculated around 4900 eV (labeled B1 and B2 as in the experiment[17]) are assigned to Ti 4p states, while the two main peaks at higher energy are associated with transitions to higher-lying states with contribu-

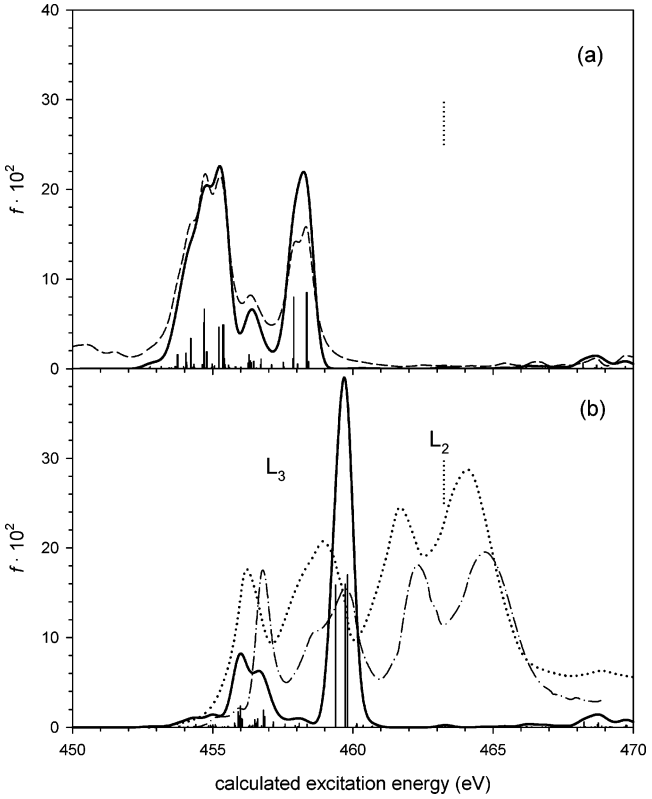

Figure 4. Ti 2p excitation spectra for the cluster $[Ti_{15}O_{40}]^{20-}$ embedded in an array of 422 PCs. Vertical dotted line, DFT-KS ionization thresholds (opposite eigenvalues): 463.232, 463.255, and 464.260 eV. Excitation profiles are convoluted with Gaussian functions (fwhm = 0.6 eV), and DOS profiles are convoluted with Lorentzian functions (fwhm = 0.6 eV). (a) Solid line, KS excitation spectra; dashed line, sum of s- and d-PDOS weighted profiles; the weight coefficients are the respective 2p → *n*s and 2p → *n*d oscillator strengths relative to the calculated transitions in the Ti^{4+} ion. DOS profiles are multiplied by 40 for best fitting calculated spectra. (b) Solid line, TDDFT spectrum; dotted line, experiment;[50] dash−dotted line, experiment.[17] Both experimental profiles are shifted along the energy axis of the same quantity, to obtain the best agreement with the calculated spectrum.

tion also from the 5p component of Ti central atom. Finally, we will comment on the results reported in panel a of Figure 3 relative to the calculation performed with the same basis set and exchange-correlation potential but at the one-electron Kohn−Sham (KS) level. As we can see, there is no substantial difference with respect to the results obtained at the correlated TDDFT level. This finding is however not surprising, since the initial Ti 1s orbital is not degenerate so only a small configuration mixing is expected from the TDDFT scheme and the simpler KS approach is suitable to properly model the K edge spectrum.

4.2. Metal L Edge Spectrum. The theoretical results concerning the Ti 2p excitations are reported in Figure 4 together with the experimental data from refs 17 and 50. In general, for the metal L edge, the main near edge structures can be explained by the dipole-allowed 2p → d transitions, and in the case of TiO_2, we have already seen that the lower-lying virtual states are mainly formed by Ti 3d and O 2p atomic components, as a result of the covalent interaction. Spin−orbit splitting of the initial 2p state results in the formation of two edges corresponding to the $2p_{1/2}$ and $2p_{3/2}$ excitations, as it is well apparent in the experimental spectrum (Figure 4) which shows two series of structures converging to L_3 and L_2 edges separated by about 5.4 eV.[17] The L_3 and L_2 lines are further split into two main components, separated by 2.5 eV, by the crystal field splitting of the excited 3d orbitals into t_{2g}- and e_g-like final orbitals.[12,17] Another splitting on the second peak of the L_3 edge is observed as a low-energy shoulder and has been related to the lower symmetry of the distorted octahedron.[17,51] The present theoretical approach does not allow the treatment of the spin−orbit effect, and it is not possible to distinguish between the L_3 and L_2 edges; therefore, we compare the TDDFT results with the experimental features converging to a single ionization threshold, generally the L_3 edge (assuming the L_2 structure as a simply broadened version of the L_3 edge). The TDDFT calculations (lower panel of Figure 4) predict the presence of two main structures, a relatively broad band of low intensity separated by about 3 eV from a sharp intense peak at higher energy. No splitting is apparent on this second structure. Note that all of the L_3 structures lie below the calculated ionization threshold. Let us consider in detail the interpretation of the theoretical results. The Ti 2p electron has dipole-allowed transitions into s and d like final states. The calculated PDOS profile of Figure 2 gives us a picture of the distribution of these levels in the cluster. The Ti 3d components give rise to a double-peaked structure in the lower-energy range of the virtual levels; it is important to note that the only other contribution to the PDOS in this energy region comes from the O 2p components. The Ti *n*s components are negligible in this energy region and appear only at higher energies. As is well-known, the transitions to *n*s states are much less intense than those to *n*d states in the L edge absorption spectra of heavier atoms[52,53] and their ratio can be estimated through the calculation of the 2p → *n*s and 2p → *n*d oscillator strengths of the metal cation Ti^{4+}. We found that the 3d/3s ratio is 89.4 in the case of Ti^{4+}, confirming that the L spectrum of TiO_2 is dominated by the d absorption channel. Multiplying the *n*s and *n*d PDOS of TiO_2 by the corresponding 2p → *n*s and 2p → *n*d oscillator strengths of the metal cation, the total PDOS reported in the upper panel of Figure 4 is obtained, which is found to approximate very well the calculated KS oscillator strengths. The shape of the low-energy d-PDOS structure reflects the distribution of the Ti 3d orbital components in the C_{2h} symmetry, which has been effectively employed in the calculations in order to account for the symmetry of the embedding charges. The energy shift between the d-PDOS peaks is about 3 eV, in agreement with previous DOS calculations[17] as well as with the experimental energy splitting of the two main L_3 components in the 2p spectrum. Following the energy level diagram reported in Figure 1, we see that the lowering of symmetry from a perfect O_h to D_{2h} (the real symmetry of rutile) up to C_{2h} causes the set of the 3d levels to split as shown. They are still distributed into two groups of MOs in the C_{2h} symmetry, which formally derive from the triply degenerate t_{2g} and doubly degenerate e_g orbitals in the O_h symmetry. However, in C_{2h}, it is no more easy to distinguish between the components of t_{2g}- and e_g-like orbitals which are distributed in the a_g and b_g MOs over the whole energy range of the 3d band (lower panel of Figure 2). The calculated KS oscillator strengths are well approximated by the d-PDOS, confirming the 3d nature of the L_3 structure.

It is interesting to compare the KS and TDDFT 2p spectra (Figure 4) in order to valuate the role of the configuration mixing. In fact, it is known that a reliable description of the 2p XAS spectrum requires the inclusion of the coupling between different excitation channels which are present in the case of 2p degenerate core holes as well as the 2p core−hole 3d electron interaction. This is correctly accounted for in the TDDFT calculations and has proven to be important in the theoretical description of the L edge.[54] There are significant differences

between KS and TDDFT spectra, in particular as concerns the intensity distribution between the two main structures; at the TDDFT level, we observe a strong reduction of the oscillator strength for the transitions contributing to the first peak and a parallel increase of the second peak, whose intensity concentrates on three main lines. The analysis of the TDDFT final states allows this behavior to be interpreted. Every final state of the first peak is described by a significant mixing of several configurations associated to transitions toward the low-lying virtual orbitals which are mainly contributed by 3d orbitals of the higher shell of Ti neighbors. The calculated oscillator strength, which directly maps the contribution to the final MOs of the 3d orbitals centered on the central Ti atom, is therefore low and is furthermore distributed over a great number of final states by the configuration mixing. Also, the small bump appearing as a higher-energy tail of the first peak can be characterized in an analogous way. This is consistent with an analysis on the electronic structure of the TiO_2 cluster in ref 21 which shows that the shells of higher shell of neighboring atoms (successive Ti shells plus surrounding oxygen atoms) strongly interact with each other and cause MOs to overlap, forming extended energy bands made up of 3d metal orbitals and 2p oxygen orbitals. The three higher-energy states of the second high structure have instead a different characterization: they are dominated by the configuration associated to the transition toward final MOs with prevalent contribution from the 3d orbitals of the Ti central atom and therefore acquire a stronger oscillator strength than the lower-energy transitions. The comparison of TDDFT results with the experiment is not quantitative, in particular as concerns the underestimate of the intensity of the first structure. We are led to ascribe this discrepancy in part to the lack of relativistic effects in the calculation; in fact, although the two components L_3 and L_2 are quite well separated, the crystal field splitting of the two main peaks (3 eV) is not very different from the spin−orbit splitting (5.4 eV). Therefore, it is expected that the spin−orbit coupling redistributes the spectral intensity over the two series of L_3 and L_2 transitions.

In summary, the configuration mixing provided by the TDDFT approach significantly redistributes the intensity of the below edge 2p transitions over fewer main lines. This behavior has also been found for the 2p metal spectra of alkaline-earth oxides.[11] The discrepancy with the experiment still present in the TDDFT results can probably be ascribed to the lack of an explicit treatment of the spin−orbit effects. For 3d systems, the L_2 and L_3 edges are in fact quite different, principally due to the coupling of the 2p core wave function and the 3d valence wave function. These effects (the so-called "multiplet effects") have the same order of magnitude of the 2p spin−orbit coupling; therefore, mixing and reordering of the $L_{2,3}$ edges occur.[55] The inclusion of the spin−orbit coupling is responsible for a redistribution of the spectral intensity over the two L_2 and L_3 series of transitions, as has been proven in the case of the $TiCl_4$ molecule for which the TDDFT approach extended to the relativistic two-component zero-order relativistic approximation (ZORA) has been employed.[56] The application of the ZORA TDDFT approach to the treatment of the 2p edge of transition metal oxides can be addressed as a future fundamental step toward a quantitative description of their XAS spectra.

We would finally comment on the further splitting (of about 1 eV) on the higher-energy peak of the L_3 edge which appears as a low-energy shoulder in the experiment.[17] In terms of a MO picture, it could represent a splitting of the e_g band due to the lowering of symmetry from O_h to D_{2h} in rutile. However, no

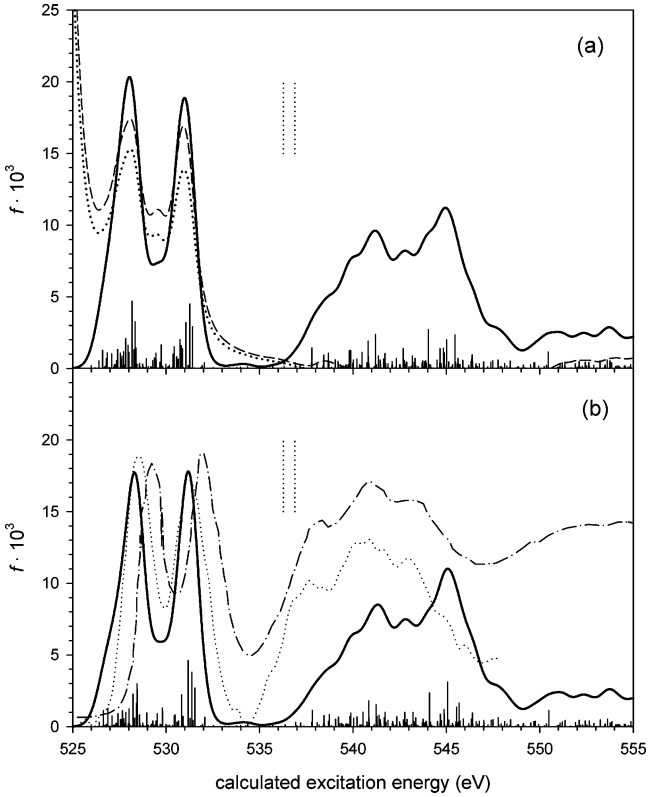

Figure 5. O 1s excitation spectra for the cluster $[Ti_{15}O_{40}]^{20-}$ embedded in an array of 422 PCs. Vertical dotted line, DFT-KS ionization thresholds (opposite eigenvalues): 536.274, 536.278, 536.283, 536.286, 536.892, and 536.896 eV. Excitation profiles are convoluted with Gaussian functions (fwhm = 1.0 eV), and DOS profiles are convoluted with Lorentzian functions (fwhm = 1.0 eV). (a) Solid line, KS spectrum; dotted line, O 2p-PDOS; dashed line, O *n*p-PDOS; PDOS profiles are multiplied by 40 for best fitting calculated spectra. (b) Solid line, TDDFT spectrum; dash−dotted line, experiment;[17] dotted line, experiment.[50] Both experimental profiles are shifted along the energy axis of the same quantity, to obtain the best agreement with the calculated spectrum.

significant splitting is discernible in our calculations nor in previous theoretical results.[17,57] Such a splitting could affect the orbital energies by less than 0.1 eV, compared with those of a perfect octahedron[57] which is too small of a value to explain the experimental result. This is in agreement with our calculations which provide a maximum splitting of 0.4 eV for the lines contributing to the higher-energy L_3 peak. Optical absorption measurements on related systems have been used to explain the "e_g splitting" in terms of a dynamic Jahn−Teller splitting, that is, the coupling of the electronic and vibrational states due to the excited state.[17,18]

4.3. Oxygen K Edge Spectrum. The KS and TDDFT theoretical results relative to the O K edge of TiO_2 are compared in Figure 5 with the experimental spectra,[17,50] in the same way as in previous figures. The experimental spectrum can be divided into two regions: the below edge one, split into two components with comparable intensities, and the above threshold region, separated by a deep minimum from the first region and extending over about 15 eV. The theoretical results reproduce correctly the two pre-edge peaks as well as the absorption profile in the higher-energy region. It has to be noted that the KS and TDDFT results are very similar; this emphasizes that the interaction of the oxygen core hole with the oxygen or titanium valence electrons can be neglected and a simple single particle scheme can be already effective for the description of the O 1s spectrum, in contrast with the Ti 2p XAS absorption. As

concerns the attribution of the structures provided by the calculations, it is worth mentioning that for the oxygen 1s edge the dipole selection rule states that only oxygen p character can be reached. In a purely ionic model for the oxide, the configuration of the oxygen is $1s^2 2s^2 2p^6$ and the $1s \rightarrow 2p$ channel would be closed in the XAS. The covalent Ti−O interaction reduces the O 2p character in the filled states so that the strength of the O 1s signal in the spectrum can be related to the degree of covalency, which is known to be quite considerable in the case of transition metal oxides. The two peaks of the pre-edge region are related to the dipole transitions to band states dominated by titanium 3d states of $t_{2g}-e_g$ symmetry separated by the "ligand field" splitting.[20] We have already emphasized the nature of these low-lying virtual orbitals discussing the Ti 2p transitions, which map the Ti 3d contribution of the conduction band, while the O 1s transitions map the O p contribution to the same virtual levels. The present calculated splitting between these two peaks is around 2.6 eV which is roughly the same value observed between the t_{2g}- and e_g-like bands in the corresponding Ti L edge spectrum. This value also closely fits the experimental one.[17] The oxygen p character of the virtual states can be inferred by the analysis of the *n*p PDOS (2p and 3p components) reported in Figure 5 (upper panel). The *n*p partial DOS is compared with the KS spectrum, which can be envisaged in a first approximation as an image of the oxygen p projected unoccupied density of states. As we can see, the partial DOS for the oxygen site shows a significant O 2p contribution in the energy region of the conduction band. A significantly lower oxygen 3p contribution is present in this energy region. The envelope of the oxygen partial DOS results in two main peaks of equal height separated by about 2.5 eV, in agreement with the KS calculated O K edge spectrum. Therefore, although the transitions involve oxygen orbitals, the below edge structure of the O 1s spectrum is determined by the electronic structure of the 3d titanium ion. The calculated intensities for the two peaks are very similar, in accord with the measured spectrum and the partial DOS. This result agrees also with the analysis of the peak intensity ratio in terms of the different hybridization of the O 2p orbitals with the t_{2g}- and e_g-like Ti d orbitals,[16,19] in particular considering the distortion of the octahedral geometry and the dispersion of the 3d titanium character over the valence band.

The second region above the threshold is characterized by a structure extending between 535 and 550 eV in our calculations which agrees well with the experimental profile, apart from an overestimate of the calculated energy separation from the below edge feature. The projected DOS reported in Figure 2 offers the possibility of analyzing the nature of virtual states falling in this region. As the energy increases, the contribution of the s and p orbitals of Ti atoms is enhanced while the contributions of p oxygen atoms significantly drops. These results are consistent with previous attribution of the above edge structure to oxygen p character hybridized with Ti 4s and 4p states of right symmetry.[19,21] Furthermore, the presence of the 4p states of the Ti atom in this energy region is the basis of the spectral assignment of the above edge structures in the Ti K edge spectrum. As we can see in Figure 5, the calculated structure is contributed by a large number of lines with low oscillator strength which is capable of mapping the small p contribution of oxygen atoms to the virtual states. In particular, the analysis of the partial DOS reveals that not only the oxygen 2p component but also the O 3p one is present in this region. More important, the O 3p character is present also at higher energy, giving rise to the tail on the higher-energy side of the above edge structure. It is important to emphasize that the high-energy range of spread of the oxygen 2p contribution to the virtual states is also indicative of the significant covalency in the TiO_2 oxide.

Finally, it is remarkable to note that the final states in all three transitions (1s, 2p, and O 1s) are the same, namely, the t_{2g}- and e_g-like antibonding orbitals. These two MOs are a combination of Ti 3d and O 2p orbitals probed by the Ti $L_{2,3}$ and O K edges, respectively; therefore, the strong calculated transition strengths account for the nature of these final states, while the relative weakness of the peaks in the Ti K edge is explained by the absence of p character in these molecular orbitals near the metal atom. The virtual states above edge also have their counterparts both in the O K edge spectrum and in the Ti K edge whose transitions map the amount of p symmetry present.

5. Conclusions

We applied the TDDFT method to the description of core excitation spectra of rutile using a cluster model to mimic the TiO_2 bulk. The Ti K and L edges and O K edge have been considered. Good agreement with experimental data has been obtained for the Ti and O K edges. The Ti K pre-edge features are discussed only in terms of dipole-allowed transitions, with the quadrupolar transitions not being included in the computational scheme; therefore, the weak A1 pre-edge structure, assigned in the literature as being quadrupolar in nature, is not present in the calculated Ti K spectrum. As concerns the Ti L edge spectrum, the configuration mixing explicitly included in the TDDFT scheme allows the metal 2p excitations for which the interaction between the degenerate 2p core states as well as the coupling of the 2p core function and the 3d valence function strongly influences the distribution of the calculated oscillator strength to be described. The discrepancies with the experiment still present in the Ti 2p TDDFT results may be associated to the lack of spin−orbit effects in the computational model.

The agreement between the TDDFT and KS results for the Ti and O K edges emphasizes instead that these edges can be correctly treated also within a simpler single particle approximation.

The spectral assignment of the various absorption features is proposed with the help of the partial density of the virtual states (PDOS) calculated for each core hole considered. The PDOS gives a graphical representation of the character of the virtual states and can be qualitatively compared with the one-electron KS spectrum.

All peaks appearing in the Ti and O K edges correspond to transitions to states which have some amount of p character mixed with 3d metal orbitals. In the case of Ti, symmetry considerations show that the 4p orbitals of the central atom can mix with d orbitals of the higher neighboring Ti in the cluster and this accounts for the low oscillator strength calculated for these transitions. In the case of the O K edge, the oxygen 2p orbitals mix with the 3d Ti orbitals and the 1s transitions are significantly higher. Then, the differences in the Ti and O spectra should arise from the outer lying atomic shells, indicating that the long range effects play an important role in the near edge structures. The Ti 2p and O 1s spectra map the content of Ti 3d and O 2p contributions, respectively, which are mixed in the low-lying virtual levels characterizing the conduction band. The relatively high oscillator strength calculated for the spectra reflects the covalent nature of the Ti−O bond in the oxide.

The present computational approach appears suitable for a realistic description of the XAS spectra of transition metal

oxides. Further improvements can be addressed for the inclusion of second-order quadrupolar transitions in the computational scheme, to account for weak intensity pre-K-edge features often observed in the case of 3d compounds, as well as for the treatment of the spin−orbit coupling in the 2p spectra of transition metals. In this way, a complete description of both L_2 and L_3 edges can be reached which represents a fundamental step toward a quantitative description of the XAS spectra. This task can be reached through the application of the ZORA TDDFT approach to the transition metal oxide clusters and is expected to require significant computational effort that we deserve for future studies.

References and Notes

(1) Batson, P. E. *Ultramicroscopy* **1993**, *78*, 33.

(2) Egerton, R. F. *Electron Energy-Loss Spectroscopy in the Electron Microscope*; Plenum Press: New York and London, 1996.

(3) de Groot, F. M. F. *Coord. Chem. Rev.* **2005**, *249*, 31.

(4) Dominguez-Ariza, D.; Sousa, C.; Illas, F.; Ricci, D.; Pacchioni, G. *Phys. Rev. B* **2003**, 68, 54101.

(5) Dominguez-Ariza, D.; Lopez, N.; Illas, F.; Pacchioni, G.; Madey, T. E. *Phys. Rev. B* **2004**, *69*, 75405.

(6) Carrasco, J.; Lopez, N.; Sousa, C.; Illas, F. *Phys. Rev. B* **2005**, *72*, 54109.

(7) Del Vitto, A.; Sousa, C.; Illas, F.; Pacchioni, G. *J. Chem. Phys.* **2004**, *121*, 7457.

(8) Stener, M.; Fronzoni, G.; de Simone, M. *Chem. Phys. Lett.* **2003**, *373*, 115.

(9) Fronzoni, G.; Stener, M.; Reduce, A.; Decleva, P. *J. Phys. Chem. A* **2004**, *108*, 8467.

(10) Stener, M.; Fronzoni, G.; De Francesco, R. *Chem. Phys.* **2005**, *309*, 49.

(11) Fronzoni, G.; De Francesco, R.; Stener, M. *J. Phys. Chem. B* **2005**, *109*, 10332.

(12) Leapman, R. D.; Grunes, L. A.; Fejes, P. L. *Phys. Rev. B* **1982**, *26*, 614.

(13) Mitterbauer, C.; Kothleitner, G.; Grogger, W.; Zandbergen, H.; Freitag, B.; Tiemeijer, P.; Hofer, F. *Ultramicroscopy* **2003**, *96*, 469.

(14) Farges, F.; Brown, G. E., Jr.; Rehr J. J. *Phys. Rev. B* **1997**, *56*, 1809.

(15) Uozumi, T.; Okada, K.; Kotani, A.; Durmeyer, O.; Kappler, J. P.; Beaurepaire, E.; Parlebas, J. C. *Europhys. Lett.* **1992**, *18*, 85.

(16) Brydson, R.; Sauer, H.; Engel, W.; Hofer, F. *J. Phys.: Condens. Matter* **1992**, *4*, 3429.

(17) Brydson, R.; Sauer, H.; Engel, W.; Thomas, J. M.; Zeitler, E.; Kosugi, N.; Kuroda, H. *J. Phys.: Condens. Matter* **1989**, *1*, 797.

(18) Brydson, R.; Williams, B. G.; Engel, W.; Sauer, H.; Zeitler, E.; Thomas, J. M. *Solid State Commun.* **1987**, *64*, 609.

(19) de Groot, F. M. F.; Faber, J.; Michiels, J. J. M.; Czyżyk, M. T.; Abbate, M.; Fuggle, J. C. *Phys. Rev. B* **1993**, *48*, 2074.

(20) de Groot, F. M. F.; Grioni, M.; Fuggle, J. C.; Ghijsen, J.; Sawatzky, G. A.; Petersen, H. *Phys. Rev. B* **1989**, *40*, 5715.

(21) Wu, Z. Y.; Ouvrard, G.; Gressier, P.; Natoli, C. R. *Phys. Rev. B* **1997**, *55*, 10382.

(22) Rez, P.; MacLaren, J. M.; Saldin, D. K. *Phys. Rev. B* **1998**, *57*, 2621.

(23) Shirley, E. L. *J. Electron Spectrosc. Relat. Phenom.* **2004**, *136*, 77.

(24) Yoshiya, M.; Tanaka, I.; Kanako, K.; Adachi, H. *J. Phys.: Condens. Matter* **1999**, *11* (16), 3217.

(25) Wu, Z. Y.; Ouvrard, G.; Natoli, C. R. *J. Phys. IV* **1997**, *7* (C2 Vol. 1), 199.

(26) Ruiz-López, M. F.; Muñoz-Páez, A. *J. Phys.: Condens. Matter* **1991**, *3*, 8981.

(27) Poumellec, B.; Durham, P. J.; Guo, G. Y. *J. Phys.: Condens. Matter* **1991**, *3*, 8195.

(28) Casida, M. E. In *Recent Advances in Density-Functional Methods*; Chong, D. P., Ed.; World Scientific: Singapore, 1995; p 155.

(29) van Gisbergen, S. J. A.; Snijders, J. G.; Baerends, E. J. *Comput. Phys. Commun.* **1999**, *118*, 119.

(30) Gross, E. K. U.; Kohn, W. *Adv. Quantum Chem.* **1990**, *21*, 255.

(31) Baerends, E. J.; Ellis, D. E.; Roos, P. *Chem. Phys.* **1973**, *2*, 41.

(32) Fonseca Guerra, C.; Snijders, J. G.; te Velde, G.; Baerends, E. J. *Theor. Chem. Acc.* **1998**, *99*, 391.

(33) van Leeuwen, R.; Baerends, E. J. *Phys. Rev. A* **1994**, *49*, 2421.

(34) Tanaka, I.; Adachi, H. *Phys. Rev. B* **1996**, *54*, 4604.

(35) Kanda, H.; Yoshiya, M.; Oba, F.; Ogasawara, K.; Adachi, H.; Tanaka, I. *Phys. Rev. B* **1998**, *58*, 9693.

(36) Stener, M.; Furlan, S.; Decleva, P. *Phys. Chem. Chem. Phys.* **2001**, *3*, 19.

(37) Stener, M.; Fronzoni, G.; Decleva, P. *Chem. Phys. Lett.* **2002**, *351*, 469.

(38) Vosko, S. H.; Wilk, L.; Nusair, M. *Can. J. Phys.* **1980**, *58*, 1200.

(39) Meagher, E. P.; George, A. L. *Can. Mineral.* **1979**, *17*, 77.

(40) Sousa, C. J.; Casanova, Rubio, J.; Illas, F. *J. Comput. Chem.* **1993**, *14*, 680.

(41) Pacchioni, G.; Ferrari, A. M.; Marq Ez, A. M.; Illas, F. *J. Comput. Chem.* **1997**, *18*, 617.

(42) Takahashi, O.; Pettersson, G. M. *J. Chem. Phys.* **2004**, *121*, 10339.

(43) Wu, Z. Y.; Zhang, J.; Ibrahim, K.; Xian, D. C.; Li, G.; Tao, Y.; Hu, T. D.; Bellucci, S.; Marcelli, A.; Zhang, Q. H.; Gao, L.; Chen, Z. Z. *Appl. Phys. Lett.* **2002**, *80* (16), 2973.

(44) Beaurepaire, E.; Lewonczuk, S.; Ringeissen, J.; Parlebas, J. C.; Uozumi, T.; Okada, K.; Kotani, A. *Europhys. Lett.* **1993**, *22*, 463.

(45) Aifa, Y.; Poumellec, B.; Jeanne-Rose, V.; Cortes, R.; Vendrinskii, R. V.; Kraizman, V. L. *J. Phys. IV* **1997**, *7* (C2 Vol. 1), 217.

(46) Poumellec, B.; Cortes, R.; Tourillon, G.; Berthon, J. *Phys. Status Solidi B* **1991**, *164*, 319.

(47) Danger, J.; Le Fevre, P.; Magnan, H.; Chandesris, D.; Bourgeois, S.; Jupille, J.; Eickhoff, T.; Drube, W. *Phys. Rev. Lett.* **2002**, *88*, 243001.

(48) Cabaret, D.; Joly, Y.; Renevier, H.; Natoli, C. R. *J. Synchrotron Radiat.* **1996**, *6*, 258.

(49) Uozumi, T.; Kotani, A.; Parlebas, J. C. *J. Electron Spectrosc.* **2004**, *137*, 623.

(50) Potapov, P. L.; Scryvers, D. *Ultramicroscopy* **2004**, *99*, 73.

(51) Scheu, C.; Gao, M.; van Benthem, K.; Tsukimoto, S.; Schmidt, S.; Sigle, W.; Richter, G.; Thomas, J. *J. Microsc.* **2003**, 210.

(52) Chaboy, J. *Solid State Commun.* **1996**, *99*, 877.

(53) Ebert, H.; Stöhr, J.; Parkin, S. S. P.; Samant, M.; Nelsson, A. *Phys. Rev. B* **1996**, *53*, 16067.

(54) Decleva, P.; Fronzoni, G.; Lisini, A.; Stener, M. *Chem. Phys.* **1994**, *186*, 1.

(55) de Groot, F. M. F.; Hu, Z. W.; Lopez, M. F.; Kaindl, G.; Guillot, F.; Tronc, M. *J. Chem. Phys.* **1994**, *101*, 6570.

(56) Fronzoni, G.; Stener, M.; Decleva, P.; Wang, F.; Ziegler, T.; van Lenthe, E.; Baerends, E. J. *Chem. Phys. Lett.* **2005**, *416*, 56.

(57) Grunes, L. A.; Leapman, R. D.; Wilker, C. N.; Hofmann, R.; Kunz, A. B. *Phys. Rev. B* **1982**, *25*, 7157.